General Synthesis and Characterization of Monocrystalline Lanthanide Orthophosphate Nanowires

Ya-Wen Zhang,[a] Zheng-Guang Yan,[a] Li-Ping You,[b] Rui Si,[a] and Chun-Hua Yan*[a]

Keywords: Nanostructures / Lanthanides / Orthophosphates / Solvothermal synthesis

Monocrystalline $LnPO_4$ (Ln = La, Ce, Pr, Nd, Sm, Eu, Gd, Tb) nanowires have been prepared in bulk quantities by a simple, facile, and clean solution-based hydrothermal method at 220–240 °C by finely tuning the acidity of the stock solutions. The length and width of the nanowires were in the range of 1–10 μm and 10–200 nm, respectively.

Introduction

In recent years, one-dimensional (1D) nanomaterials such as nanowires, nanobelts, nanotubes, and nanorods have attracted growing interest not only because of their unique properties with respect to their bulk materials, but also because of their promising applications in mesoscopic physics and fabrication of nanodevices of electronics, optoelectronics, and biochemical sensing.[1−9] Among the 1D nanomaterials, nanowires have played key roles as both interconnectors and active components in fabricating the nanodevices.[1,2,5] Therefore, to synthesize diverse nanowires with well-controlled shape, size, phase purity, crystallinity, and chemical composition on a large scale has become one of the most challenging issues faced by synthetic inorganic chemists.[10] So far, a rich variety of nanowires such as elemental semiconductors, II−VI and III−V semiconductors, metal oxides, and metals have been prepared by methods including templating direction, catalytic growth, electrochemistry, chemical vapor deposition, and solution-based solvothermal or hydrothermal treatment.[1−4]

Based on the electronic, optical, and chemical characteristics originating from their unique 4*f* electron configurations, lanthanides have promised various applications in magnets, phosphors, catalysts, biochemical probes, and medical diagnostics, and thus are of rapidly growing importance. In lanthanide chemistry, much of the recent attention has been focused on the fields of the coordination chemistry of lanthanides, organic transformations mediated or catalyzed by rare-earth compounds, and the preparation and properties of new lanthanide-related materials.[11] More recently, some lanthanide-related materials (oxides, borates, and fluorides) were reported to show exceptional electrical or luminescent behaviors when their grain sizes were reduced to the nanometer regime.[12−14] Nevertheless, the advance in the studies of 1D-nanostructured rare earth related compounds is still very limited, only nanowires/nanotubes of rare earth hydroxides/oxides have been prepared and characterized.[15−18] Amongst the large number of lanthanide inorganic salts, lanthanide phosphates are widely used in the production of luminescent or laser materials, moisture sensors, heat-resistant materials, and hosts for radioactive nuclear waste.[19−23] In this paper, we will report the general synthesis of monocrystalline lanthanide orthophosphate nanowires by a solution-based hydrothermal route by finely tuning the acidity of the stock solutions.

Lanthanide orthophosphates with the chemical formula $LnPO_4{\cdot}nH_2O$ ($n = 0-3$) (Ln^{3+} = lanthanide ion) have five polymorphs: monazite (monoclinic), xenotime (tetragonal), rhabdophane (hexagonal), weinschenkite (monoclinic), and orthorhombic.[23] In this research, $LnPO_4{\cdot}nH_2O$ ($n = 0-0.5$) were hydrothermally prepared at 220−240 °C for 17−24 h, using H_3PO_4, $NH_4H_2PO_4$, $(NH_4)_2HPO_4$, $(NH_4)_3PO_4$, or their mixtures, as both the precipitators and the mediators of acidity. Experimentally, monazite-type $LnPO_4$ (Ln = La, Ce, Pr, Nd, Sm, Eu, Gd) nanowires, rhabdophane-type $TbPO_4{\cdot}0.5H_2O$ nanowires/nanorods, and xenotime-type $LnPO_4$ (Ln = Dy, Ho, Er, Tm, Yb, Lu, Y) nanocrystals were obtained.

Results and Discussion

The crystal structures of the products have been identified by X-ray diffraction analysis (XRD). In Figure 1(a), we show the typical XRD pattern of the $LaPO_4$ nanowires. All the reflections can be distinctly indexed to a pure mono-

[a] State Key Laboratory of Rare Earth Materials Chemistry and Applications, PKU-HKU Joint Laboratory in Rare Earth Materials and Bioinorganic Chemistry, Peking University, Beijing 100871, China
Fax: (internat.) + 86-10-62754179
E-mail: chyan@chem.pku.edu.cn
[b] Electron Microscopy Laboratory
Peking University, Beijing 100871, China

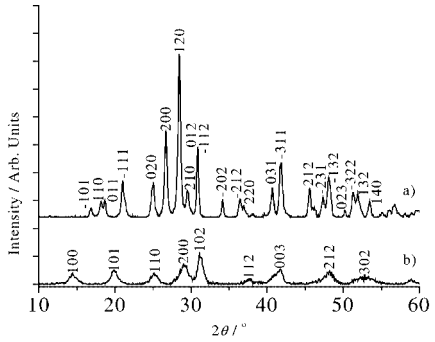

Figure 1. XRD patterns of $LaPO_4$: (a) nanowires; (b) colloidal precipitate

clinic phase (space group $P2_1/n$) with lattice constants a = 6.868 Å, b = 7.104 Å, c = 6.521 Å, and β = 103.6° (JC,PDS No. 32-493). Such a monoclinic structure was also identified for the other $LnPO_4$ nanowires. From Figure 1(b), we noted that the $LaPO_4$ colloid precipitate prior to hydrothermal treatment shows a hexagonal structure (JC,PDS No. 46-1439) and consists of nanoparticles as suggested by the line broadening of the diffraction peaks. The XRD pattern shown in Figure 2 informs us that the $TbPO_4{\cdot}0.5H_2O$ product is of hexagonal structure (space group $P3_121$) with lattice constants a = 6.799 Å and c = 6.332 Å (JC,PDS No. 20-1244). XRD analysis also showed that the as-synthesized $LnPO_4$ products of heavy lanthanides exhibit a zircon-type structure with tetragonal symmetry (space group $I4_1/amd$) with grain sizes in the range of 20−150 nm, as estimated by transmission electron microscopy (TEM).

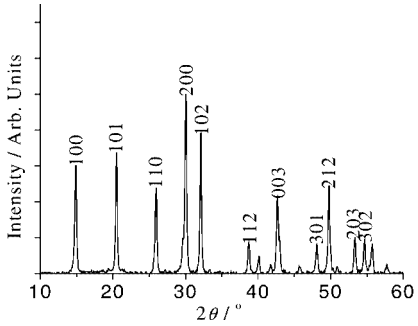

Figure 2. XRD pattern of $TbPO_4{\cdot}0.5H_2O$ nanowires/nanorods

By TEM and high resolution TEM (HRTEM), the morphology, crystallinity, and growth directions of the nanowires were carefully examined. From Figure 3, we can see that the as-prepared monoclinic $LnPO_4$ nanowires have a length of between 1 and 10 μm and a width of between 10 and 200 nm, are pure without any appreciable amount of particulate by-products, and are of a single-crystal nature. The surfaces of the nanowires are perfect without any stacking faults, and clean without any sheathed amorphous phase even at the edges. The preferred growth direction of the monazite-type nanowires was determined along the c axis [001]. Figure 4 shows that the $TbPO_4{\cdot}0.5H_2O$ nanowires/nanorods are perfect single crystals with a length of between 0.5 and 2 μm and a width of between 20 and

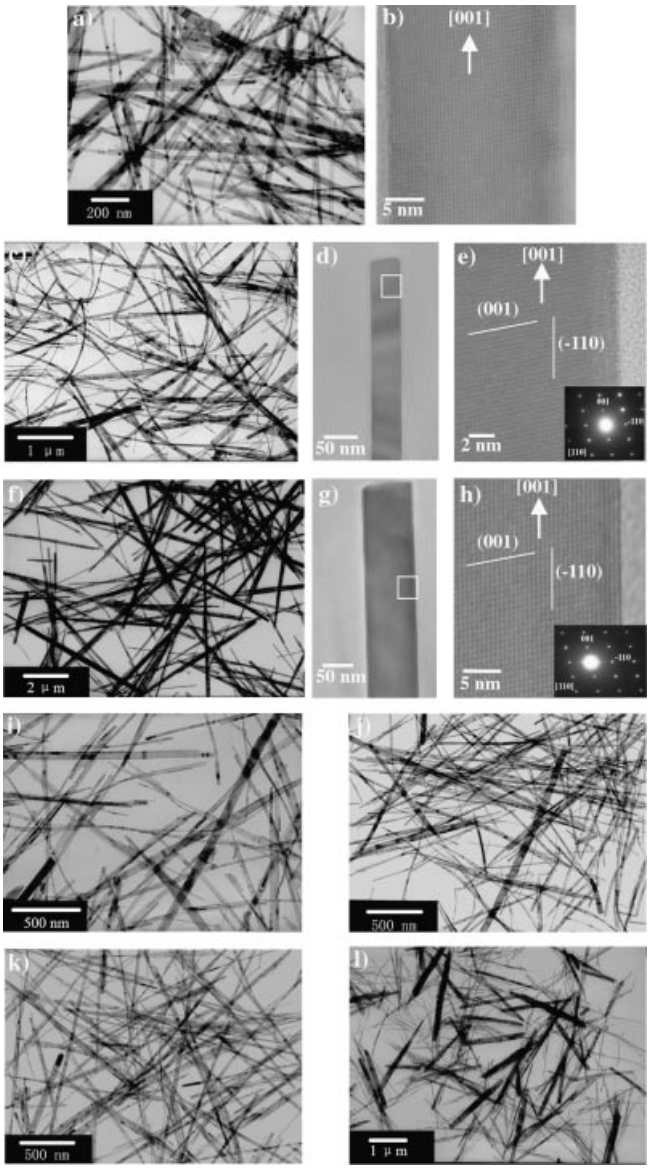

Figure 3. (a) TEM image of $LaPO_4$ nanowires; (b) HRTEM image of a single 23 nm $LaPO_4$ nanowire; (c) TEM image of $SmPO_4$ nanowires; (d) TEM image of a uniform 50 nm $SmPO_4$ nanowire; (e) HRTEM image of a single $SmPO_4$ nanowire taken from the highlighted section with inset showing the electron diffraction pattern; (f) TEM image of $EuPO_4$ nanowires; (g) TEM image of a uniform 80 nm $EuPO_4$ nanowire; (h) HRTEM image of a single $EuPO_4$ nanowire taken from the highlighted section with inset showing the electron diffraction pattern; (i) TEM image of $CePO_4$ nanowires; (j) TEM image of $PrPO_4$ nanowires; (k) TEM image of $NdPO_4$ nanowires; and (l) TEM image of $GdPO_4$ nanowires/nanorods

150 nm. The HRTEM image and selected area electron diffraction (SAED) pattern shown in Figure 4(b) and (c), respectively, suggest that the $TbPO_4{\cdot}0.5H_2O$ single crystals also grow along the c axis. From Figures 3 and 4, we can see that the nanowires of light lanthanides are more uniform than those of middle lanthanides, possibly resulting from the differences in their intrinsic properties such as solubility, ionic mobility and growth rate in solution associated with the lanthanide contraction.[24] In addition, the smooth morphology and perfect monocrystalline nature of

the as-synthesized nanowires indicate that a reversible pathway between the solution phase and the solid phase, which allows building blocks in $LnPO_4$ crystals to adopt the correct positions, was established during the hydrothermal treatment employed. The optimal preparative conditions, crystal structures, length, and width of the $LnPO_4$ nanowires are summarized in Table 1.

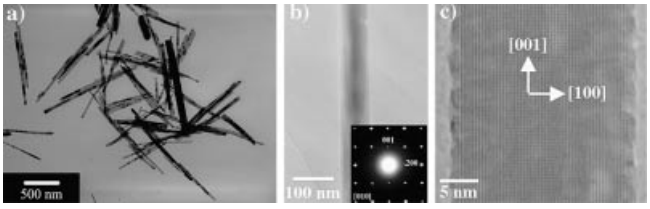

Figure 4. (a) TEM image of $TbPO_4 \cdot 0.5H_2O$ nanowires/nanorods; (b) TEM image of a uniform 70 nm $TbPO_4 \cdot 0.5H_2O$ nanorod with inset showing the electron diffraction pattern; and (c) HRTEM image of a single 25 nm $TbPO_4 \cdot 0.5H_2O$ nanowire

Solution-based hydrothermal/solvothermal methods have already become a commonly used methodology for preparing shaped/sized/oriented nanomaterials, but a quantitative thermodynamic prediction of the crystallization in the nanometer regime for growing 1D nanomaterials by this method is still very difficult and requires extensive research.[2] Herein, the preferred growth direction of the $LnPO_4$ nanowires was understood from the viewpoint of energy by simulating the coordination fashion of the rare earth ions in the monazite structure based on the Kossel model of crystal growth on completely smooth surfaces.[25] As is well-known, the lanthanide atoms in the monazite structure are coordinated to nine oxygen atoms forming a polyhedron of pentagonal interpenetrating tetrahedra, and the nine-coordinate lanthanide atoms are apically combined by the distorted tetrahedral PO_4^{3-} groups forming chains.[26] Figure 5 shows the growth models of $LaPO_4$ nanowires along the [001] (*c* axis) and [100] (*a* axis) directions, which were constructed using the CERIUS2 software package.[27] From Figure 5(a), we can see that two La−O bonds form as a PO_4^{3-} tetrahedron is attached along the [001] direction. However, only one La−O bond forms when

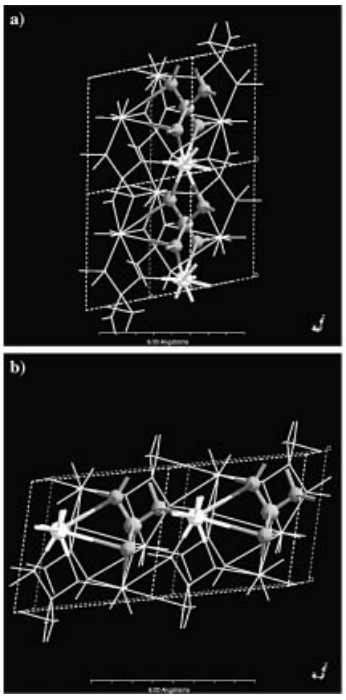

Figure 5. Growth models for $LaPO_4$ along different directions built up by CERIUS2 software: (a) [001] and (b) [100]

the growth is along the [100] direction (Figure 5, b). The growth along the [001] direction can release more energy, and the La−O bond lengths in the two cases show slight differences.[26] Thus, the [001] direction should be preferably taken when $LnPO_4$ nanowires are growing. Moreover, it is inferred that the anisotropic nature of the building blocks in the monazite structure should be one source of the driving forces for the growth of the $LnPO_4$ nanowires.

Control experiments were carried out to screen the optimal conditions for preparing phase-pure monocrystalline $LnPO_4$ nanowires. It was shown that the temperature and the starting acidity in the mother liquors are the major factors governing the crystallinity and the phase purity of the products. Temperature-dependent experiments showed that pure dehydrated monocrystalline nanowires could only be prepared at temperatures above 200 °C, and the dehydration temperature for middle lanthanides is higher than that for light lanthanides. When heat-treated at 220−240

Table 1. Optimal preparative conditions, crystal structures and morphologies of the $LnPO_4$ nanowires

Sample	Preparative conditions		Structure	Morphology	
	pH	Temperature [°C]		Length [μm]	Width [nm]
$LaPO_4$	0.8	220	monoclinic	1−3	20−50
$CePO_4$	0.8	220	monoclinic	2−5	20−100
$PrPO_4$	0.8	220	monoclinic	1−4	10−60
$NdPO_4$	0.8	220	monoclinic	1−3	20−60
$SmPO_4$	0.8	220	monoclinic	2−6	50−150
$EuPO_4$	1	240	monoclinic	3−10	50−200
$GdPO_4$	2	240	monoclinic	1−3	20−200
$TbPO_4 \cdot 0.5H_2O$	1.6	240	hexagonal	0.5−2	20−150

°C, $LnPO_4$ (Ln = La, Pr, Nd, Sm, Eu) products exhibit the monazite structure under the acidities investigated. However, at the same temperatures, pure monazite $CePO_4$ could only be synthesized at pHs less than 1. When the pH is greater than 1, cubic CeO_2 will coexist with monazite-type $CePO_4$ due to the partial oxidization of Ce^{3+} at the reduced acidity in solution. Pure monazite-type $GdPO_4$ instead of mixed phases of rhabdophane and monazite could only be prepared at pHs between 1.5 and 6 at 240 °C. In the case of $TbPO_4$, no monazite phase was obtained under the acidities used at 240 °C; instead, pure rhabdophane and xenotime phase were obtained at pHs greater than 1.5 and lower than 1.5, respectively.

At a given heat-treatment temperature, it was observed that the morphologies of the products depend strongly upon the starting acidity and the formation of colloidal precipitates in the mother liquors. As an example, the effects of the preparative conditions on the morphologies of the $LaPO_4$ products are given in Table 2. It can be seen that $LaPO_4$ nanowires could only be obtained in a fairly narrow pH range (between 0.5 and 1.5) in the presence of the colloidal precipitate. In fact, the acidity of the stock solutions was finely tuned according to the following equation:

$$Ln^{3+} + (NH_4)_mH_{3-m}PO_4 \rightarrow LnPO_4 \downarrow + (3 - m)\cdot H^+ + m\cdot NH_4^+ \quad (m = 0-3)$$

The hexagonal $LaPO_4$ colloidal precipitate was confirmed to be an aggregate of nearly spherical nanoparticles with sizes around 80 nm (Figure 6). Those nanoparticles could serve as anisotropic seeds for the growth of highly anisotropic nanostructures in the solution solid process by a dissolution and crystallization mechanism during the hydrothermal treatment employed.[15,28,29] At pH values between 0.8 and 6, the colloidal precipitate formed instantly in the stock solution. After hydrothermal treatment, the morphologies of the $LaPO_4$ products changed from nanoparticles/nanorods (at pH 6, Figure 7, a) to nanowires/nanorods (at pH 1.6, Figure 7, b), then to nanowires (at pH 0.8−1.3, Figures 3 and 7, a and c, respectively), along with the increasing aspect ratio (also see Table 2). When the starting acidity of the stock solution was further enhanced by the addition of H_3PO_4, the colloidal precipitate formed gradually over a few minutes or even disappeared. After hydrothermal treatment, the morphologies of the $LaPO_4$ products changed from nanowires (at pH 0.8−1.3, Figures 3 and 7, a and c, respectively) to nanowires/nanorods (at 1 mol·L^{-1} H_3PO_4, Figure 7, d), then to nanorods (at 2 mol·L^{-1} H_3PO_4, Figure 7, e), along with the decreasing aspect ratio (see also Table 2).

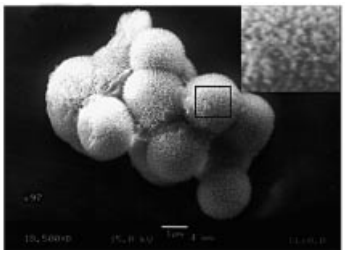

Figure 6. SEM images at different magnifications of the $LaPO_4$ colloidal precipitate prepared at pH 0.8 (inset was taken from the highlighted section)

Previously, Peng et al. have investigated the effects of chemical potential on the shape evolution of CdSe nanocrystals with the wurtzite structure, and observed that the high chemical potential generated by a high monomer concentration in the growth solution favors the growth of elongated nanocrystals.[30] Very recently, Li et al. found that a higher chemical potential was a dominant driving force for the growth of hexagonal lanthanide hydroxide nanowires during hydrothermal treatment.[15] In the present case, the concept of chemical potential was also used to explain the above experimental phenomenon related to the formation of $LnPO_4$ nanowires. We think that the chemical potential of the monoclinic $LnPO_4$ crystals is mainly determined by the apparent concentration of $LnPO_4$ in the solutions, which depends thermodynamically upon the acidity of the reaction system. Previously, the apparent solubility of $LnPO_4$ in aqueous solution was found to decrease upon increasing the precipitation temperature.[31] Under mild to strongly acidic conditions, the apparent concentration of $LnPO_4$ in boiling H_3PO_4 solution decreases gradually upon increasing the concentration of H_3PO_4 from 0.5 to 2 M, and decreases drastically when it is higher than 2 M.[31] Under weakly acidic conditions, Ln^{3+} ions are known to hydrolyze slightly in solution with the formation of both mononuclear and polynuclear species in small amounts before the precipitation of the hydroxide occurs above pH 6.[32] In ad-

Table 2. Effect of the preparative conditions on the morphologies of the $LaPO_4$ products prepared at 220 °C for 17 h

Acidity	Precipitating[a]	Morphology Length [μm]	Width [nm]	
pH = 6	instantly	0.05−0.2	10−20	nanoparticles/nanorods
pH = 1.6	instantly	0.2−0.7	10−60	nanowires/nanorods
pH = 1.3	instantly	0.5−3	30−70	nanowires
pH = 1	instantly	1−3	20−90	nanowires
pH = 0.8	instantly	1−3	20−50	nanowires
1 mol·L^{-1} H_3PO_4	gradually	0.1−0.3	20−200	nanowires/nanorods
2 mol·L^{-1} H_3PO_4	−	0.08−0.3	40−100	nanorods
4 mol·L^{-1} H_3PO_4	−	0.04−0.12	50−300	nanorods

[a] Formation of colloidal precipitates before hydrothermal treatment.

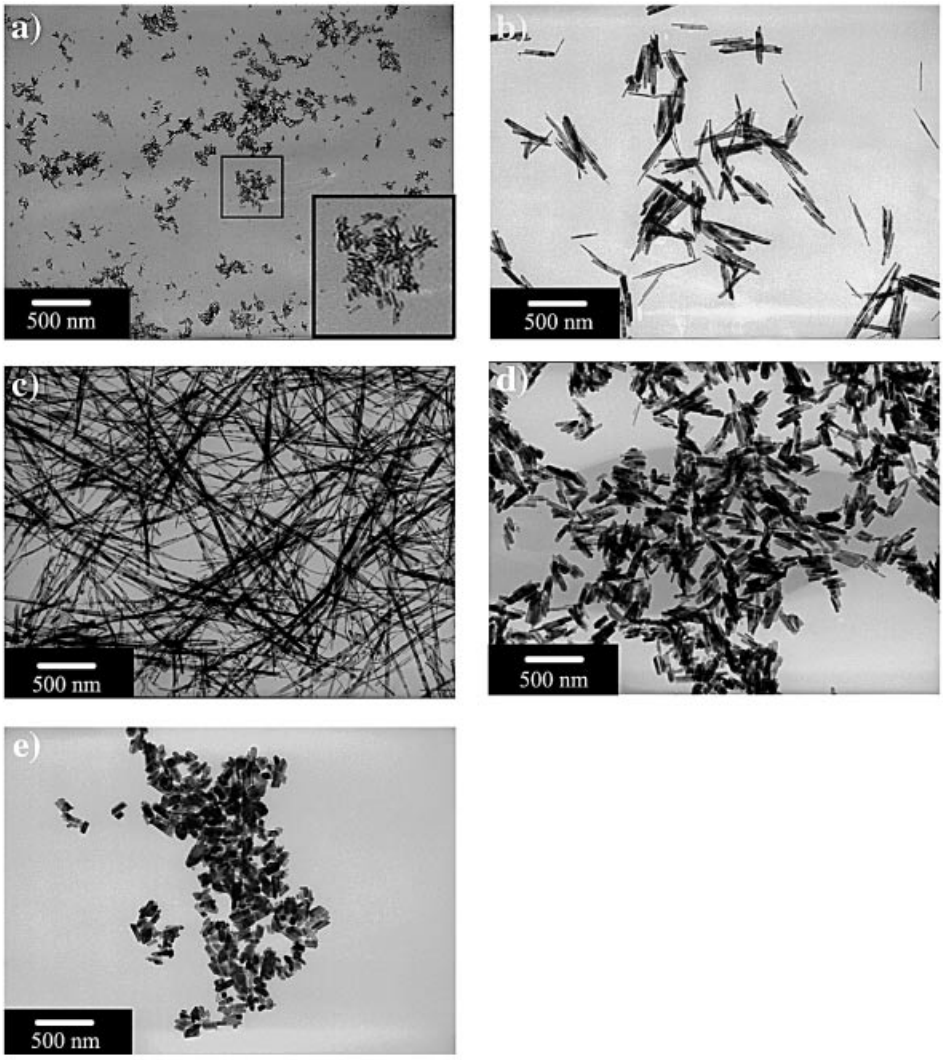

Figure 7. TEM images of the hydrothermal products of $LaPO_4$ prepared at 220 °C for 17 h: (a) pH 6 (inset was taken from the highlighted section); (b) pH 1.6; (c) pH 1.3; (d) 1 mol·L^{-1} H_3PO_4; (e) 2 mol·L^{-1} H_3PO_4

dition, the hydrolysis rate increases with pH value. In the present experiments, both the increasing hydrolysis of La^{3+} ions at pH values greater than 1.5 and the increasing acidity by addition of H_3PO_4 ($\geq$ 0.5 M) are thought to reduce the apparent concentration of $LaPO_4$ and thus its chemical potential in solution. As a result, the $LaPO_4$ nanowires could only be prepared in a fairly narrow pH range (0.5−1.5) where the chemical potential of $LaPO_4$ crystals is higher. Interestingly, the coexistence of the $LaPO_4$ nanorods/nanoparticles (at pH 6, Figure 7, a) or nanowires/nanorods (at pH 1.6 or at 1 M H_3PO_4, Figure 7, b and d) might indicate the mixed-shape evolution of 1D/2D ripening.[30] Conclusively, a high chemical potential of $LnPO_4$ crystals in solution should be another major driving force for the growth of the $LnPO_4$ nanowires.

As demonstrated above by XRD analysis, there is a structural transition from monazite to rhabdophane, then to xenotime with the ionic radius of Ln^{3+} decreasing from La to Lu, and rhabdophane-type $TbPO_4$ sits on the borderline for this transition. Under the synthetic conditions investigated, we found that $LnPO_4$ with larger Ln^{3+} ions could be synthesized in the form of nanowires at suitable pH values, whereas $LnPO_4$ with the heavier and smaller Ln^{3+} ions could only be prepared in the form of nanocrystals. This result might hint that xenotime-type $LnPO_4$ crystals have lower structural anisotropy and lower chemical potential in solution than monazite-type $LnPO_4$ crystals, probably as a result of their lower coordination number and increasing solubility induced by the lanthanide contraction.[31,33] In the xenotime-type structure, Ln ions are eight-coordinate to oxygen atoms from the somewhat-distorted tetrahedral PO_4^{3-} groups to form a polyhedron of bis-bisphenoid.[33]

Conclusion

We have demonstrated the general synthesis of $LnPO_4$ monocrystalline nanowires in bulk quantities and high purity by a simple, facile, and clean solution-based hydrothermal method by finely tuning the acidity of the stock solu-

tions. This successful demonstration can assist us to understand the fundamentals of the reaction and nanowire growth mechanisms under hydrothermal conditions. Our recent experiments also showed that monocrystalline rhabdophane and orthorhombic hydrated $LnPO_4$ 1D nanomaterials and luminescent-active $LaPO_4$:Eu and $LaPO_4$:CeTb nanowires can be also prepared by the same synthetic approach. It is expected that the hydrothermal route employed in this work can be extended to the preparation of other pure and doped 1D nanomaterials with highly anisotropic structures. Moreover, the as-synthesized monocrystalline lanthanide orthophosphate nanowires may promote both academic interest in lanthanide chemistry and novel applications in nanotechnology. Further research on the luminescent behavior of doped $LnPO_4 \cdot nH_2O$ 1D nanomaterials associated with the reduced dimensionality are in progress.

Experimental Section

Synthesis of the $LnPO_4$ Nanowires: Quantitative solutions of $Ln(NO_3)_3$ (AR, > 99.9%) and H_3PO_4 [$NH_4H_2PO_4$/$(NH_4)_2HPO_4$/$(NH_4)_3PO_4$ or their mixtures] of analytical grade in a given molar ratio (usually 1:1.1) were employed to prepare a stock solution (40 mL) with a cation concentration of 0.05 M in a Teflon cup (50 mL). After 15 min of stirring, the cup was transferred into a stainless steel autoclave, and subjected to hydrothermal treatment at 220−240 °C for 17−24 h under autogenous pressure in an electric oven. As the autoclave cooled to room temperature, precipitates with the color of lanthanide ions were formed and collected. The precipitates were washed with deionized water, centrifugally filtered off, and dried at 60 °C for 24 h. The yields of the products were about 80−90%.

The water content in the products was determined with a thermogravimetry and differential thermal analyzer (Du Pont 2100) in air at a heating rate of 10 °C/min, using α-Al_2O_3 as a reference. The crystal structures of the products were obtained on a powder X-ray diffractometer (Rigaku D/max-2000, Japan), employing Cu-K_α radiation (λ = 1.5418 Å). The sizes and morphologies of the products were characterized by scanning electron microscopy (AMARY 1910FE, USA) at 15 kV, transmission electronic spectroscopy (200CX, JEOL, Japan) at 160 kV and high-resolution transmission electronic spectroscopy (H-9000, Hitachi, Japan) at 400 kV.

Acknowledgments

Grants-in-aids from NSFC (Nos. 20171003, 20221101, 50272006, and 20023005), MOST of China (G19980613), and Founder Foundation of Peking University are gratefully acknowledged.

[1] J. T. Hu, T. W. Odom, C. M. Lieber, *Acc. Chem. Res.* **1999**, *32*, 435−445.
[2] Y. N. Xia, P. D. Yang, Y. G. Sun, Y. Y. Wu, B. Mayers, B. Gates, Y. D. Yin, F. Kim, H. Q. Yan, *Adv. Mater.* **2003**, *15*, 353−389.
[3] Y. Y. Wu, H. Q. Yan, M. Huang, B. Messer, J. H. Song, P. D. Yang, *Chem. Eur. J.* **2002**, *8*, 1260−1268.
[4] G. R. Partzke, F. Krumeich, R. Nesper, *Angew. Chem. Int. Ed.* **2002**, *41*, 2446−2461.
[5] X. F. Duan, Y. Hang, R. Agarwal, C. M. Lieber, *Nature* **2003**, *421*, 241−245.
[6] M. S. Arnold, P. Avouris, Z. W. Pan, Z. L. Wang, *J. Phys. Chem. B* **2003**, *107*, 659−663.
[7] R. Martel, T. Schmidt, H. R. Shea, T. Hertel, Ph. Avouris, *Appl. Phys. Lett.* **1998**, *73*, 2447−2449.
[8] S. J. Trans, R. M. Verschueren, C. Dekker, *Nature* **1998**, *393*, 49−52.
[9] S. S. Wong, E. Joselevich, A. T. Woolley, C. L. Cheung, C. M. Lieber, *Nature* **1998**, *394*, 52−55.
[10] Y. N. Xia, P. D. Yang, *Adv. Mater.* **2003**, *15*, 351−352.
[11] H. B. Kagan, *Chem. Rev.* **2002**, *102*, 1805−1806.
[12] Y. W. Zhang, Y. Yang, S. Jin, S. J. Tian, G. B. Li, J. T. Jia, C. S. Liao, C. H. Yan, *Chem. Mater.* **2001**, *13*, 372−378.
[13] Z. G. Wei, L. D. Sun, C. S. Liao, J. L. Yin, X. C. Jiang, C. H. Yan, S. Z. Lu, *J. Phys. Chem. B* **2003**, *106*, 10610−10617.
[14] J. W. Stouwdam, F. C. J. M. van Veggel, *Nano Lett.* **2002**, *2*, 733−737.
[15] X. Wang, Y. D. Li, *Angew. Chem. Int. Ed.* **2002**, *41*, 4790−4793.
[16] A. W. Xu, Y. P. Fang, L. P. You, H. Q. Lin, *J. Am. Chem. Soc.* **2003**, *125*, 1494−1495.
[17] C. F. Wu, W. P. Qin, G. S. Qin, D. Zhao, J. S. Zhang, S. H. Huang, S. Z. Lu, H. Q. Liu, H. Y. Lin, *Appl. Phys. Lett.* **2003**, *82*, 520−522.
[18] M. Yada, M. Mihara, S. Mouri, M. Kuroki, T. Kijima, *Adv. Mater.* **2002**, *14*, 309−313.
[19] K. Riwotzki, H. Meyssamy, H. Schnablegger, A. Kornowski, M. Haase, *Angew. Chem. Int. Ed.* **2001**, *40*, 573−576.
[20] K. Riwotzki, H. Meyssamy, A. Kornowski, M. Haase, *J. Phys. Chem. B* **2000**, *104*, 2824−2828.
[21] H. Meyssamy, K. Riwotzki, *Adv. Mater.* **1999**, *11*, 840−844.
[22] S. Nishihama, T. Hirai, I. Komasawa, *J. Mater. Chem.* **2002**, *12*, 1053−1057.
[23] H. Ito, Y. Fujishiro, T. Sato, A. Okuwaki, *Br. Ceram. Trans.* **1995**, *94*, 146−150.
[24] N. N. Greenwood, A. Earnshaw, *Chemistry of the Elements*, 2nd ed.; Oxford: Butterworth-Heinemann, **1998**, p.1235−1237.
[25] A. W. Vere, *Crystal Growth, Principles and Progress*, Plenum, New York, **1987**, p. 14−15.
[26] D. F. Mullica, W. O. Milligan, D. A. Grossie, G. W. Beall, L. A. Boatner, *Inorg. Chim. Acta* **1984**, *95*, 231−236.
[27] http://www.accelrys.com/cerius2
[28] B. Gates, Y. D. Yin, Y. N. Xia, *J. Am. Chem. Soc.* **2000**, *122*, 12582−12583.
[29] J. Lu, Y. Xie, F. Xu, L. Y. Zhu, *J. Mater. Chem.* **2002**, *12*, 2755−2761.
[30] Z. A. Peng, X. G. Peng, *J. Am. Chem. Soc.* **2001**, *123*, 1389−1395.
[31] R. Kijkowska, *J. Mater. Sci.* **2003**, *38*, 229−233.
[32] C. F. J. Baes, R. E. Mesmer, *The Hydrolysis of Cations*, John Wiley & Sons, New York, **1976**, p. 129−146.
[33] W. O. Milligan, D. F. Mullica, G. W. Beall, L. A. Boatner, *Inorg. Chim. Acta* **1982**, *60*, 39−43.

Received June 25, 2003

